International Journal of Pharmaceutics 416 (2011) 365–375

Contents lists available at ScienceDirect

International Journal of Pharmaceutics

journal homepage: www.elsevier.com/locate/ijpharm

Pharmaceutical Nanotechnology

Transport of saquinavir across human brain-microvascular endothelial cells by poly(lactide-*co*-glycolide) nanoparticles with surface poly-(γ-glutamic acid)

Yung-Chih Kuo*, Hsin-Wei Yu

Department of Chemical Engineering, National Chung Cheng University, Chia-Yi 62102, Taiwan, ROC

ARTICLE INFO

Article history:
Received 8 April 2011
Received in revised form 27 May 2011
Accepted 22 June 2011
Available online 28 June 2011

Keywords:
Blood–brain barrier
Poly-(γ-glutamic acid)
Poly(lactide-*co*-glycolide)
Human brain-microvascular endothelial cell
Human astrocyte
Saquinavir

ABSTRACT

Poly(lactide-*co*-glycolide) (PLGA) nanoparticles (NPs) with surface poly-(γ-glutamic acid) (γ-PGA) were applied to enhance the transport of saquinavir (SQV) across the blood–brain barrier (BBB). PLGA NPs encapsulated SQV and grafted with γ-PGA to form drug carriers (γ-PGA/SQV-PLGA NPs) for crossing through a monolayer of human brain-microvascular endothelial cells (HBMECs) regulated with human astrocytes. The results revealed that a lower molecular weight of γ-PGA yielded a higher grafting efficiency of γ-PGA on PLGA NPs. In addition, γ-PGA with a low molecular weight accelerated the dissolution of SQV from γ-PGA/SQV-PLGA NPs. A higher grafting efficiency (more didecyl dimethylammonium bromide) and a lower molecular weight of γ-PGA increased the permeability of SQV across the BBB, in general. When the grafting efficiency was 85.2% at 6 kDa of γ-PGA, γ-PGA/SQV-PLGA NPs reached about 6 times the permeability of free SQV (the maximal permeability). γ-PGA could also promote the endocytosis of NPs and expression of ornithine decarboxylase by HBMECs. γ-PGA/SQV-PLGA NPs are efficacious nanoparticulate carriers in delivering antiretroviral drug across the BBB.

Nomenclature

D	cumulant *Z*-average diameter (nm)
$GE_{\gamma\text{-PGA}}$	grafting efficiency of γ-PGA on SQV-PLGA NPs (%)
$\langle GE_{\gamma\text{-PGA}} \rangle$	average grafting efficiency of γ-PGA on SQV-PLGA NPs (%)
$MW_{\gamma\text{-PGA}}$	viscosity average molecular weight of γ-PGA (kDa)
$P_{\text{HBMEC/HA}}$	permeability of SQV across a monolayer of HBMECs regulated by HAs (cm/s)
P_{SQV}	cumulative weight percentage of SQV released from γ-PGA/SQV-PLGA (%)
t	dissolution time (day)
ζ	zeta potential (mV)

1. Introduction

An innovated design of polymeric colloids for drug delivery is one of the most focused issues in bionanotechnology. In addition to polymers, many types of materials, such as inorganic nanoparticles (NPs), solid lipid NPs, dentrimers, nanotubes, and liposomes, have been used as drug carriers (Date et al., 2007; Faraji and Wipf, 2009; Junghanns and Müller, 2008). The intriguing motif of this approach is based on the hypothesis that the biomaterial particles imitate pathogens and can be identified, phagocytosed, and processed by antigen-presenting cells. Several synthetic biopolymers, such as poly(lactide-*co*-glycolide) (PLGA) and poly(ε-caprolactone), were fabricated for the delivery of pharmaceuticals (Hans and Lowman, 2002). In addition, biodegradable poly-(γ-glutamic acid) (γ-PGA), a natto mucilage from certain strains of *Bacillus subtilis*, has been developed since the late 1960s (Kunioka and Furusawa, 1997). The biosynthetic process of γ-PGA is normally distinguished by whether γ-glutamic acid is an essential nutrient (Ito et al., 1996). In biomedical application, γ-PGA NPs have been used in immobilizing ovalbumin and maintaining the viability of HL-60 cells (Akagi et al., 2005). γ-PGA NPs were also potent vaccine vehicles to deliver antigenic proteins and inhibit ovalbumin-transfected tumors (Yoshikawa et al., 2008). An incorporation of γ-PGA NPs into hemagglutinin vaccine could promote the immune responses for protection against influenza virus (Okamoto et al., 2009). Moreover, γ-PGA could facilitate the dissociation of chitosan and deoxyribonucleic acid and increase

Abbreviations: BBB, blood–brain barrier; BMEC, brain-microvascular endothelial cell; DDAB, didecyl dimethylammonium bromide; HA, human astrocyte; HBMEC, human brain-microvascular endothelial cell; HBMEC/HA, HA-regulated HBMECs; NP, nanoparticle; ODC, ornithine decarboxylase; PLGA, poly(lactide-*co*-glycolide); SQV, saquinavir; SQV-PLGA, SQV-encapsulated PLGA; γ-PGA, poly-(γ-glutamic acid); γ-PGA/PLGA, γ-PGA-grafted PLGA; γ-PGA/SQV-PLGA, γ-PGA-grafted SQV-PLGA.

* Corresponding author. Tel.: +886 5 272 0411x33459; fax: +886 5 272 1206.
E-mail address: chmyck@ccu.edu.tw (Y.-C. Kuo).

0378-5173/$ – see front matter © 2011 Elsevier B.V. All rights reserved.
doi:10.1016/j.ijpharm.2011.06.037

the cellular internalization of extracellular substances (Peng et al., 2009). Furthermore, γ-PGA improved the cellular internalization of materials via γ-PGA-specific receptor-mediated pathway (Kurosaki et al., 2010). The particle uptake was also regulated by γ-PGA-specific receptor-mediated process with energy-dependent characteristics (Kurosaki et al., 2009).

The medicinal treatment concerning drug delivery across the blood–brain barrier (BBB) is a critical challenge in the present stage (Kuo and Chen, 2006; Schroeder et al., 1998). For example, the inhibition to the growth of human immunodeficiency virus (HIV) requires the transport of curatives into the brain parenchyma where HIV resides (Glynn and Yazdanian, 1998). In fact, enhancing the permeability of antiretroviral drug across the BBB can ameliorate the virus-inducing disorders in the central nervous system (CNS). However, the manufacturing practice seldom offers answers to the delivery and cell uptake of therapeutic reagents. On the contrary, a BBB model using proper cells can benefit the assessment of CNS-targeting drugs (Kreuter, 2005; Kuo and Chung, 2005). The main cellular component of the BBB is brain-microvascular endothelial cells (BMECs), which are the foremost sentinels of the CNS. When BMECs propagated on a porous membrane, the confluent monolayer resembles the feature of the BBB *in vivo* (Gaillard and de Boer, 2000; Kuo and Kuo, 2008). The properties of the BBB preserved in an *in vitro* model include a typical endothelial morphology, expression of endothelial markers such as CD51, CD62P, CD71, and cadherin, localization of marginal filamentous actin, expression of tight junction, expression of γ-glutamyl transpeptidase, expression of P-glycoprotein, transmembrane delivery of transferrin, restricted paracellular transport, and high transendothelial electrical resistance (TEER). Besides BMECs, astrocytes also play an important role in the tissue site of the BBB (Pardridge, 2005). More than 90% astrocyte end-feet surround BMECs to regulate signal transmission and mediate the transport of metabolites and essential nutrients (Deeken and Löscher, 2007). A monolayer of human BMECs (HBMECs) regulated with human astrocyte (HA) (defined as HBMEC/HA) could demonstrate a TEER about 230 Ω cm^2 and permeability of propidium iodide about 4×10^{-6} cm/s (Kuo and Lu, 2011a). This suggested that HBMECs and HAs can construct an appropriate BBB model.

The aim of this study is to investigate the delivery of saquinavir (SQV) across the BBB using a carrier system of γ-PGA-grafted SQV-PLGA NPs (γ-PGA/SQV-PLGA NPs). SQV is one of the important protease inhibitors to inhibit HIV growth. γ-PGA was synthesized by fermentation of *Bacillus licheniformis* ATCC 9945a and decomposed thermally into polymers with smaller molecular weight. The morphology of γ-PGA/SQV-PLGA NPs, particle size distribution, average particle size, zeta potential, grafting efficiency of γ-PGA, release kinetics of SQV, permeability of SQV across the BBB, uptake of NPs, and expression of ornithine decarboxylase (ODC) were studied.

2. Materials and methods

2.1. Biosynthesis of γ-PGA

γ-PGA was prepared by a biosynthetic process using *B. licheniformis* ATCC 9945a (BCRC, Hsin-Chu, Taiwan). Cryopreserved *B. licheniformis* was unfrozen and cultivated by streak culture containing agar (Sigma, St. Louis, MO). Single colony about 1 mm^2 in the streak culture was grazed along, mixed with 5 mL of liquid medium containing 0.375% (w/v) beef extract (BD Bacto, Franklin Lakes, NJ) and 0.625% (w/v) peptone (Sigma), and incubated in a shaking flask at 150 rpm and 37 °C for 24 h. The cultivated *B. licheniformis* in the suspension was mixed with 20 mL of production medium containing 2% (w/v) L-glutamic acid (Sigma), 1.2% (w/v) citric acid (Sigma), 8% (w/v) glycerol (Sigma), 0.7% (w/v) NH_4Cl (Sigma), 0.05% (w/v) $MgSO_4 \cdot 7H_2O$ (J.T. Baker, Phillipsburg, NJ), 0.004% (w/v) $FeCl_3 \cdot 6H_2O$ (Sigma), 0.05% (w/v) K_2HPO_4 (Riedel-de Haen, Seelze, Germany), 0.015% (w/v) $CaCl_2 \cdot 2H_2O$ (Sigma), and 0.0104% (w/v) $MnSO_4 \cdot H_2O$ (Sigma). This formulation was cultivated at 150 rpm and 37 °C for 48 h. Then, the suspension was added with 10 mL of the production medium and cultivated again at 150 rpm and 37 °C for 24 h. Finally, 70 mL of the production medium was added and the cultivation continued for another 24 h. The sticky fluid was poured out into a sterile conical tube (50 mL, Falcon, Franklin Lakes, NJ) and centrifuged by a refrigerated ultracentrifuge (Optima LE-80K, Beckman Coulter, Fullerton, CA) at 20,000 × *g* and 4 °C for 30 min. One aliquot of the supernatant was mixed with four aliquots of ethanol (95%, Taiwan Sugar Corporation, Tainan, Taiwan), placed in a refrigerator at 4 °C overnight, and centrifuged at 20,000 × *g* and 4 °C for 30 min. Coarse γ-PGA in the pellet was washed with ultrapure water (Barnstead, Dubuque, IA), centrifuged at 20,000 × *g* and 4 °C for 30 min, and purified using a dialysis bag (12.4 kDa) pretreated with ethylene-diamine-tetra-acetic acid (EDTA, Riedel-de Haen) in a flask of 500 mL containing 200 mL of ultrapure water at 150 rpm and 37 °C for 1 h. The dialyzed γ-PGA in 10 mL of the fluid was dissolved in 40 mL of ultrapure water at 150 rpm and 25 °C, mixed with 8 mL of hydrochloric acid (Riedel-de Haen), and stirred at 150 rpm and 25 °C for 6 h. Fine γ-PGA was collected after vacuum filtration, washed with ultrapure water, and dried in an oven at 50 °C for 6 h.

2.2. Thermal decomposition of γ-PGA and determination of molecular weight

100 mg γ-PGA was dissolved in 100 mL of ultrapure water, thermally decomposed in a batch reactor (Chan-Ja Automatic, Tainan, Taiwan) with 1 L of reaction tank at 150 rpm and 150 °C for 1, 3, and 5 h, and centrifuged at 20,000 × *g* and 4 °C for 30 min. The bottom pellet was collected. The viscosity average molecular weight of the degraded γ-PGA, M_v, was determined by the following Mark–Houwink equation (Irurzun et al., 2001):

$$[\eta] = 4.1 \times 10^{-5} \cdot M_v^{0.94}$$

where $[\eta]$ is the intrinsic viscosity and can be estimated by

$$[\eta] = \lim_{C \to 0} \frac{\eta_{sp}}{C} = \lim_{C \to 0} \frac{\ln \eta_r}{C}$$

$$\eta_{sp} = \frac{\eta - \eta_{s,\gamma}}{\eta_{s,\gamma}}$$

$$\eta_r = \frac{\eta}{\eta_{s,\gamma}}$$

In these expressions, η_{sp}, η_r, η, $\eta_{s,\gamma}$, and C are, respectively, the specific viscosity, the relative viscosity, the viscosity of water, the viscosity of the suspension containing γ-PGA, and the concentration of γ-PGA. $\eta_{s,\gamma}$ of the polymer suspension containing 0.01, 0.02, 0.03, 0.04, and 0.05% (w/v) γ-PGA was obtained by a MCR 500 rheometer (Anton Paar, Graz, Austria) at a shear rate of 10 s^{-1} using US 200 software. An extrapolation on the series data of η_{sp} to C approaching zero yielded $[\eta]$.

2.3. Fabrication of γ-PGA/SQV-PLGA NPs

SQV-PLGA NPs were prepared by emulsification-diffusion method. 20 mg PLGA (Purac, Bingen, Germany) and 2 mg SQV ($C_{38}H_{50}N_6O_5$, MW 670.841, United States Pharmacopeial, Rockville, MD) were dissolved in 20 mL of propylene carbonate (PC, Sigma) at 400 rpm and 25 °C for 1 h. SQV-free PLGA

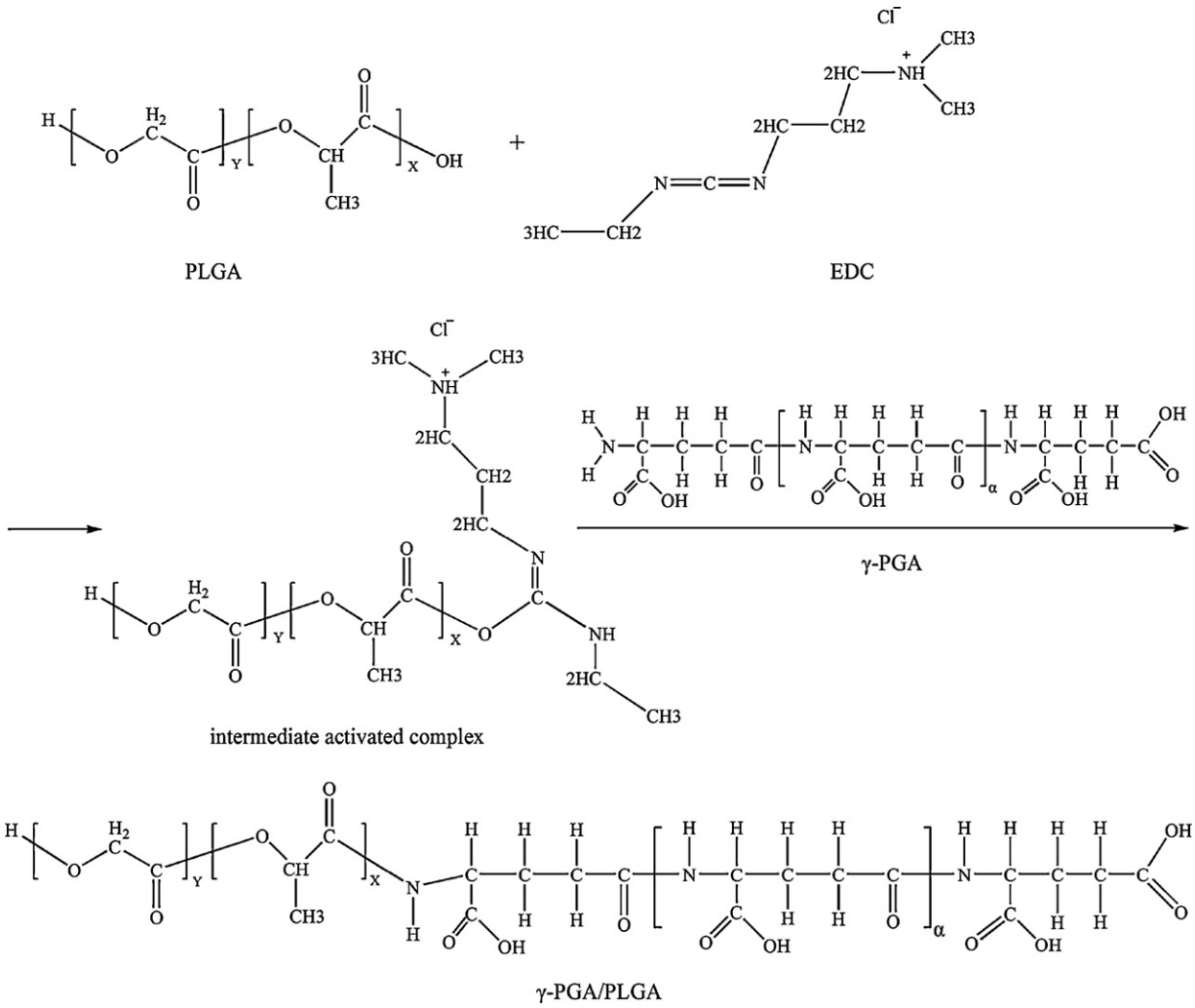

Fig. 1. Reaction mechanism of γ-PGA grafted on SQV-PLGA NPs.

NPs were prepared without the addition of 2 mg SQV in PC. In addition, fluorescent carriers were synthesized by dissolving 0.1 mg fluorescein isothiocyanate-dextran (Sigma) with PLGA and SQV in PC. 12–48 mg didecyl dimethylammonium bromide (DDAB, Sigma) and 0.4–1.6 mg 1,2-distearoyl-sn-glycero-3-phosphoethanolamine-N-[carboxy(polyethylene glycol)-2000] (DSPE-PEG(2000)-carboxylic acid, Avanti Polar Lipid, Alabaster, AL) (3.34% (w/w) DDAB) were mixed in 40 mL of ultrapure water at 400 rpm and 25 °C for 1 h. The two solutions were emulsified by a homogenizer (PT 2100, Kinematica AG, Lucerne, Switzerland) at 30,000 rpm and 25 °C for 10 min. The aqueous phase containing DDAB and DSPE-PEG(2000)-carboxylic acid was added gradually into the homogenizer within 5 min. 140 mL of ultrapure water was added into the microemulsion at 1000 rpm and 25 °C for 1 h. These DDAB-stabilized SQV-PLGA NPs were dialyzed 10 times in a dialysis bag of 12.4 kDa for 1 h. The dialysate was analyzed by a high performance liquid chromatography (HPLC, Jasco, Tokyo, Japan) with a UV–visible detector (UV-2075 Plus, Jasco, Tokyo, Japan) at 239 nm. The mobile phase containing a gradient of acetonitrile (BDH, Poole, England) from 5 to 45% with a flow rate of 0.85 mL/min for 20 min was driven by two high-pressure pumps (PU-2080 Plus, Jasco, Tokyo, Japan) in series. The entrapment efficiency of SQV in PLGA NPs was defined as [(total weight of SQV − weight of free SQV)/(total weight of SQV)] × 100% (Kuo, 2005). In this formulation, the entrapment efficiency was 77.38 ± 2.98%.

The dialyzed SQV-PLGA NPs were filtrated through a filtration paper with pores of 1 μm. The filtrate was centrifuged by a superspeed refrigerated centrifuge (AVANTij-25, Beckman Coulter) at 159,000 × *g* and 4 °C for 10 min. The bottom pellet was resuspended in ultrapure water containing 2% (w/v) D-mannitol (Sigma), frozen in an ultralow temperature freezer at −80 °C for 30 min, and lyophilized by a freeze dryer (Eyela, Tokyo, Japan) at 2–4 Torr and −80 °C over 24 h. The powders of SQV-PLGA NPs were stored at 4 °C.

0.01% (w/v) SQV-PLGA NPs, 0.096% (w/v) 1-ethyl-3-(3-dimethylaminopropyl) carbodiimide (EDC, Sigma), and 0.023% (w/v) N-hydroxysuccinimide (NHS, Acros, Morris, NJ) were mixed at 150 rpm and 25 °C for 4 h (Kuo et al., 2009). The EDC-activated SQV-PLGA NPs were crosslinked with 0.005% (w/v) γ-PGA at 150 rpm and 25 °C for 4 h. The suspension was centrifuged at 159,000 × *g* and 4 °C for 1 h. The pellet containing γ-PGA/SQV-PLGA NPs was collected and dried at 50 °C. Fig. 1 shows the reaction mechanism for synthesizing γ-PGA/PLGA NPs. Fig. 2 illustrates the structure of γ-PGA/SQV-PLGA NP. The supernatant containing free γ-PGA was mixed with ethanol at 4 °C overnight and centrifuged at 20,000 × *g* and 4 °C for 1 h. Solid γ-PGA at the bottom was dried and weighed. The grafting efficiency of γ-PGA on SQV-PLGA NPs, $GE_{\gamma\text{-PGA}}$, was calculated by $GE_{\gamma\text{-PGA}}$ = [(total weight of γ-PGA − weight of free γ-PGA)/(total weight of γ-PGA)] × 100%.

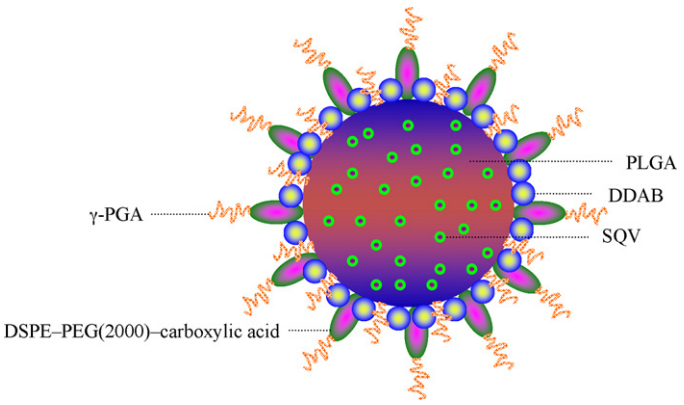

Fig. 2. Schematic structure of γ-PGA/SQV-PLGA NP.

2.4. Characterization

The particle size distribution, cumulant *Z*-average diameter (*D*), and zeta potential (*ζ*) of γ-PGA/SQV-PLGA NPs were analyzed by a zetasizer 3000 HS_A (Malvern, Worcestershire, UK) with a photon correlation spectroscope connected with a laser Doppler velocimeter at 25 °C. The concentration of γ-PGA/SQV-PLGA NPs in 0.1 M Tris buffer (Riedel-de Haen) was 0.2 mg/mL. The colloidal suspension was injected gradually into a quartz tube to avoid the formation of bubbles. Measuring the particle size distribution and average diameter required 2 min, and measuring the zeta potential required 20 s.

A field emission scanning electron microscope (FE-SEM, JSM-6330 TF, Jeol, Tokyo, Japan) was employed to study the surface of γ-PGA/SQV-PLGA NPs. The samples were vacuum-dried and sputter-coated with platinum with accelerating voltage of 2 kV for 90 s. In addition, these polymeric particles were loaded on a carbon-coated 200-mesh copper grid for 2 min before visualization by a transmission electron microscope (TEM, JEM-1400, Jeol, Tokyo, Japan). The samples were treated with 2% (w/v) phosphotungstic acid solution (Sigma) for 2 min to negatively stain the highly electron-transmissible atoms.

The molecular weight of γ-PGA/PLGA NPs was analyzed by gel permeation chromatography (GPC). An HPLC pump (model 510, Waters, Milford, MA) was applied to impel the mobile phase containing tetrahydrofuran (J.T. Baker) in a column set of WAT044230 HR05, WAT044221 HR3, WAT044225 HR4, and WAT044227 HR5 for separating the dissolved polymers. A tunable absorbance UV–visible detector (Waters 486, Waters) was used to estimate the absorbance of eluted polymers.

2.5. Dissolution of SQV from γ-PGA/SQV-PLGA NPs

0.2% (w/v) γ-PGA/SQV-PLGA NPs was resuspended in Dulbecco's phosphate buffered saline (DPBS, Sigma) containing 0.05% (w/v) sodium azide (Sigma) as a biocide at pH 7.4. 10 mL of the suspension was added into an EDTA-pretreated dialysis bag of 12.4 kDa, placed in a flask of 100 mL containing 40 mL of DPBS, and shaken in a bath-reciprocal shaker at 50 rpm and 37 °C over 31 days. 100 μL of the sample containing released SQV was analyzed by the HPLC followed with the UV detector at 239 nm. The liquid volume in the flask was maintained at 40 mL by immediate compensation with 100 μL of fresh DPBS at the specific sampling points. The cumulative percentage of SQV released, P_{SQV}, was evaluated by P_{SQV} (%) = [(cumulative weight of SQV in dissolution medium)/(total weight of SQV in γ-PGA/SQV-PLGA NPs)] × 100%.

2.6. HA-regulated monolayer of HBMECs

HAs (Sciencell, Corte Del Cedro Carlsbad, CA) propagated in an incubator (NuAire, Plymouth, MN) with an atmosphere of 95% relative humidity and 5% CO_2 at 37 °C over 7 days. The seeding density of HAs was 7500 cells/cm^2 on T75 tissue culture flask (Corning Costar, Cambridge, MA) with pretreated human fibronectin (Sigma). The culture medium for HAs was astrocyte medium (Sciencell) containing astrocyte growth supplement (Sciencell) at a replacement rate of every 2 days. After washed with DPBS, the expanded HAs were separated with trypsin-EDTA (Sigma), washed with DPBS, and centrifuged at 150 × *g* for 5 min. The excess HAs in the culture medium containing 10% (v/v) dimethyl sulfoxide (J.T. Baker) and 10% (v/v) fetal bovine serum (FBS, Biocompare) were frozen in a refrigerator at 4 °C for 1 h, in a low temperature freezer (Frigidaire, Augusta, GA) at −20 °C for 1 h, and in an ultralow temperature freezer at −80 °C for 1 h and then stored in liquid nitrogen. A brief protocol for propagating HBMECs (Biocompare, South San Francisco, CA) was described previously (Kuo and Chen, 2007).

The expended HAs were seeded on the bottom surface of sterilized polyethylene terephthalate (PET) membrane (cell culture insert, pore size 1.0 μm, BD, Franklin Lakes, NJ) with a density of 4×10^5 cells/cm^2 in an inverted transwell system and cultivated in the CO_2 incubator for 1 h. The top surface of the PET membrane was seeded with the expended HBMECs with a density of 4×10^5 cells/cm^2. Both surfaces of the PET membrane were pretreated with human fibronectin. This HBMEC/HA transwell system was placed in a 12-well microtiter plate (Corning Costar) and cocultivated in the CO_2 incubator over 14 days to form a confluent monolayer of HBMECs regulated with HAs. The lower (outer) chamber was filled with the culture medium of HAs. The medium in the upper (inner) chamber for culturing HBMECs was endothelial cell medium (ECM, Biocompare) containing 1% endothelial cell growth supplement (Biocompare), 5% FBS and 1% penicillin/streptomycin solution (Biocompare). Both media were replaced at a rate of every 2 days and maintained at the same height to shun the effect of hydrostatic pressure on HBMECs and HAs.

2.7. Permeability across cocultured HBMEC/HA system

The PET membrane with the cultured HBMEC/HA system was fixed between two chambers containing 14 mL of DPBS each. Both chambers were maintained at 37 °C by circulating water around their external jacket and stirred at 150 rpm. The donor and receiver chambers faced HBMECs and HAs, respectively. 0.065% (w/v) γ-PGA/SQV-PLGA NPs were added into the donor chamber. The concentration of SQV was controlled between 98% and 102% of its initial level in the donor chamber throughout an independent experiment over 3 h. 50 μL of the fluid in the receiver chamber was drawn out every 20 min, mixed with 450 μL of acetone (Mallinckrodt Baker, Hazelwood, MO) at 50 rpm and 25 °C for 5 min to dissolve SQV from γ-PGA/SQV-PLGA NPs, and analyzed by the HPLC-UV scheme at 239 nm. The medium volume in the receiver chamber was compensated with 50 μL of fresh DPBS when sampling. The permeability coefficient of SQV across the HA-regulated monolayer of HBMECs ($P_{HBMEC/HA}$) was calculated by $1/P_{HBMEC/HA} = 1/P_e - 1/P_m$, where P_e and P_m are the permeability of SQV across the PET membrane containing HBMEC/HA and the permeability of SQV across the PET membrane, respectively.

2.8. Uptake of particles and expression of ODC

HBMECs (200 μL) with a density of 1×10^5 cells/mL were seeded on a pretreated cover slip in 24-well microtiter plate (Falcon), cultivated in the CO_2 incubator at 37 °C for 8 h, and treated with 0.065% (w/v) fluorescent γ-PGA/SQV-PLGA NPs for 1.5 h. The cells were

fixed with 4% (v/v) formalin (Sigma) at 4 °C for 5 min, immersed in 0.5% (v/v) Triton-X-100 (Acros) at 25 °C for 5 min, incubated with serum blocking solution (Zymed, South San Francisco, CA) at 25 °C for 1 h, treated with ODC1 rabbit anti-human polyclonal antibody (Abcam, Cambridge, MA) in a dilution ratio of 1:300 at 4 °C for 16 h, and reacted with Alexa Fluor® 555 goat anti-rabbit IgG (H + L) (Invitrogen, Carlsbad, CA) in a dilution ratio of 1:300 at 25 °C for 1 h. The nuclei of HBMECs were stained with 50% (w/v) 4′,6-diamidino-2-phenylindole (Sigma) at 25 °C for 10 min. The fluorescent images were visualized by a confocal laser scanning microscope (LSM 510, Zeiss, Oberkochen, Germany) in excitation wavelengths at 555 nm (red), 458 nm (green), and 380 nm (blue), and emission wavelengths at 565 nm (red), 488 nm (green), and 460 nm (blue) (Kuo and Chiu, 2011). The images were analyzed by Image-Pro Plus (version 4.5, Media Cybernetics, Bethesda, MD) in the red-green-blue color model with red between 54 and 90, green between 120 and 180, and blue between 210 and 255.

2.9. Statistics

Data presented were mean ± standard deviation. Statistical significance between two groups of data was assessed using a one-way analysis of variance (ANOVA) followed by Tukey's HSD test.

3. Results and discussion

Fig. 3(1) shows the particle size distribution of γ-PGA/SQV-PLGA NPs with three molecular weights of the grafted γ-PGA. In this figure, the molecular weights of γ-PGA in (a), (b), and (c) are 6, 14, and 52 kDa, respectively. As indicated in Fig. 3(1), these drug carriers displayed a typical trait of normal distribution in particle size. When the molecular weight of γ-PGA was 6 and 14 kDa, the suspended γ-PGA/SQV-PLGA NPs were closed to monodispersed colloids with small polydispersity index of 0.002. A relatively wide range of the particle size was detected when the molecular weight of γ-PGA was 52 kDa. The rationale behind this result is that the extensibility of the hydrophilic γ-PGA chain is high in aqueous milieu. Therefore, γ-PGA with the molecular weight of 52 kDa expanded randomly on the surface of SQV-PLGA NPs and yielded a comparably broad particle size distribution. As revealed in Fig. 3(1), the *Z*-average particle diameter of γ-PGA/SQV-PLGA NPs was 188.8 nm for γ-PGA of 6 kDa, 218.1 nm for γ-PGA of 14 kDa, and 307.6 nm for γ-PGA of 52 kDa. This indicated that an increment in the molecular weight of γ-PGA increased the particle size of γ-PGA/SQV-PLGA NPs. The explanation for these results was that an increment in the molecular weight of γ-PGA enhanced the swollen capability of γ-PGA and promoted the space occupation of γ-PGA into nearby surroundings. Fig. 3(2) shows the SEM images of γ-PGA/SQV-PLGA NPs with 6 kDa of γ-PGA in (a), 14 kDa in (b), and 52 kDa in (c). As displayed in this figure, γ-PGA/SQV-PLGA NPs were easy to condense and demonstrated strongly interconnected clusters after drying. This was because the shrinkage of surface γ-PGA produced an adherent force among the polymeric colloids (Kreuter, 2001). In addition, these particles exhibited spheroid-like exteriors. Fig. 3(3) shows the TEM results corresponding to Fig. 3(1) and (2) (also corresponding to the different molecular weights of γ-PGA in (a), (b), and (c)). As indicated in Fig. 3(3), the dark cores were SQV-PLGA NPs. These dark zones were similar in magnitude because SQV-PLGA NPs were formed first and the surface coating of γ-PGA followed (Kuo and Lin, 2009; Langer et al., 1996). The gray layers around SQV-PLGA NPs were the grafted γ-PGA. As compared with the strong staining of SQV-PLGA NPs, the appearance of the light staining of γ-PGA resulted from the loose configuration of γ-PGA on the particulate surface. In the TEM imaging, isolated γ-PGA/SQV-PLGA NPs were selected in order to obtain clear particle boundaries. Therefore, Fig. 3(3) demonstrated a different particle exterior from the partly coalescent clusters shown in Fig. 3(2).

Fig. 4 shows the variation in the average particle diameter of γ-PGA/SQV-PLGA NPs as a function of the weight percentage of DDAB. As revealed in this figure, the average particle diameter increased with increasing the molecular weight of γ-PGA at a fixed concentration of DDAB. This resulted from the extended surface layer of γ-PGA (see the discussion in Fig. 3(1)). In fact, the particle size of SQV-PLGA NPs increased when γ-PGA was linked on the surface via amide bond (–CONH–). As indicated in Fig. 4, an increase in the concentration of DDAB increased the average particle diameter at a fixed molecular weight of γ-PGA (6, 14, or 52 kDa). The rationale behind this trend was described as follows. First, the dissociation of proton from carboxyl group enabled γ-PGA to carry negative charge. Second, the adherent positive charge of DDAB on SQV-PLGA NPs attracted γ-PGA (Fasbender et al., 1997; Kuo and Yu, 2011). As a result, a higher concentration of DDAB led to a larger adsorbed quantity of DDAB on SQV-PLGA NPs, attracted more γ-PGA to the surface of SQV-PLGA NPs, and increased the particle size of γ-PGA/SQV-PLGA NPs. In addition, the average particle diameter enhanced noticeably when the concentration of DDAB increased from 0.02 to 0.06%. This increase in the particle size became obscure when the concentration of DDAB increased from 0.06 to 0.08%. These results suggested that the grafted quantity of γ-PGA approached saturation when the concentration of DDAB was about 0.06–0.08% (data shown in Fig. 6).

Fig. 5 shows the effect of the molecular weight of γ-PGA and the weight percentage of DDAB on the zeta potential of γ-PGA/SQV-PLGA NPs. As revealed in this figure, an increment in the molecular weight of γ-PGA, from 6 kDa, increasing to 14 kDa and then 52 kDa, reduced the absolute value of the zeta potential. The factors affecting the surface charge of γ-PGA/SQV-PLGA NPs were explained as follows. First, the exposed carboxyl groups of γ-PGA obtained a higher chance to dissociate protons. Second, the surface charge on DDAB-stabilized SQV-PLGA NPs was reversed by the modification of γ-PGA, i.e., from positive to negative charge (Chung et al., 2007; Kuo and Chung, 2011). Third, the proportion of exposed carboxyl groups in γ-PGA with a low molecular weight was larger than that with a high molecular weight. Fourth, based on the same weight of γ-PGA, the negative charge grafted onto SQV-PLGA NPs using a low molecular weight of γ-PGA was larger than that using a high molecular weight of γ-PGA. Therefore, γ-PGA with a low molecular weight demonstrated a higher ability in grafting negative charge than γ-PGA with a high molecular weight. As indicated in Fig. 5, an increase in the weight percentage of DDAB enhanced the absolute value of the zeta potential. This was because a higher quantity of the adherent DDAB attracted a higher quantity of γ-PGA to the particle surface, rendering a larger negative charge on γ-PGA/SQV-PLGA NPs (Sonorhara et al., 1995; Kuo and Lin, 2006). When the weight percentage of DDAB increased from 0.02 to 0.06%, an obvious enhancement in the absolute value of the zeta potential appeared. The enhancement in the absolute value of the zeta potential became unclear when the weight percentage of DDAB increased from 0.06 to 0.08%. These results were consistent with Fig. 4 and could be related to the grafting efficiency of γ-PGA (data shown in Fig. 6).

Fig. 6 shows the grafting efficiency of γ-PGA on the surface of SQV-PLGA NPs in response to the varied molecular weight of γ-PGA and weight percentage of DDAB. As indicated in this figure, an increment in the molecular weight of γ-PGA reduced the grafting efficiency of γ-PGA. This was because a graft with a higher molecular weight of γ-PGA produced a stronger steric repulsion and decreased the recruitment capacity for additional free γ-PGA. As revealed in Fig. 6, an increase in the weight percentage of DDAB enhanced the grafting efficiency of γ-PGA. The reason for this outcome was that a higher weight percentage of DDAB attracted more

γ-PGA via electrical interaction (Kuo and Lin, 2008; Makino et al., 1994). However, the increase in the grafting efficiency was vague when the weight percentage of DDAB increased from 0.06 to 0.08%. This suggested that the occupation of γ-PGA on SQV-PLGA NPs approached a completion at about 0.06–0.08% DDAB. This phenomenon was consistent with the results shown in Figs. 4 and 5.

Fig. 7 shows the typical GPC peak of γ-PGA/PLGA NPs. As revealed in this figure, the average retention time was about 21.04 min. The number and weight average molecular weight were 97,176 and 102,299 Da, respectively. Thus, the polydispersity was about 1.0527. In addition, the peak molecular weight was 103,405 Da. The weight average molecular weight of PLGA upon purchase was about 100 kDa. Based on the results, the grafting of γ-PGA on the surface of PLGA NPs could only insignificantly affect the molecular weight of γ-PGA/PLGA NPs.

Fig. 8 shows the dissolution kinetics of SQV from γ-PGA/SQV-PLGA NPs. As revealed in this figure, the initial 5 days were the first burst stage of release. The existence of this stage suggested an

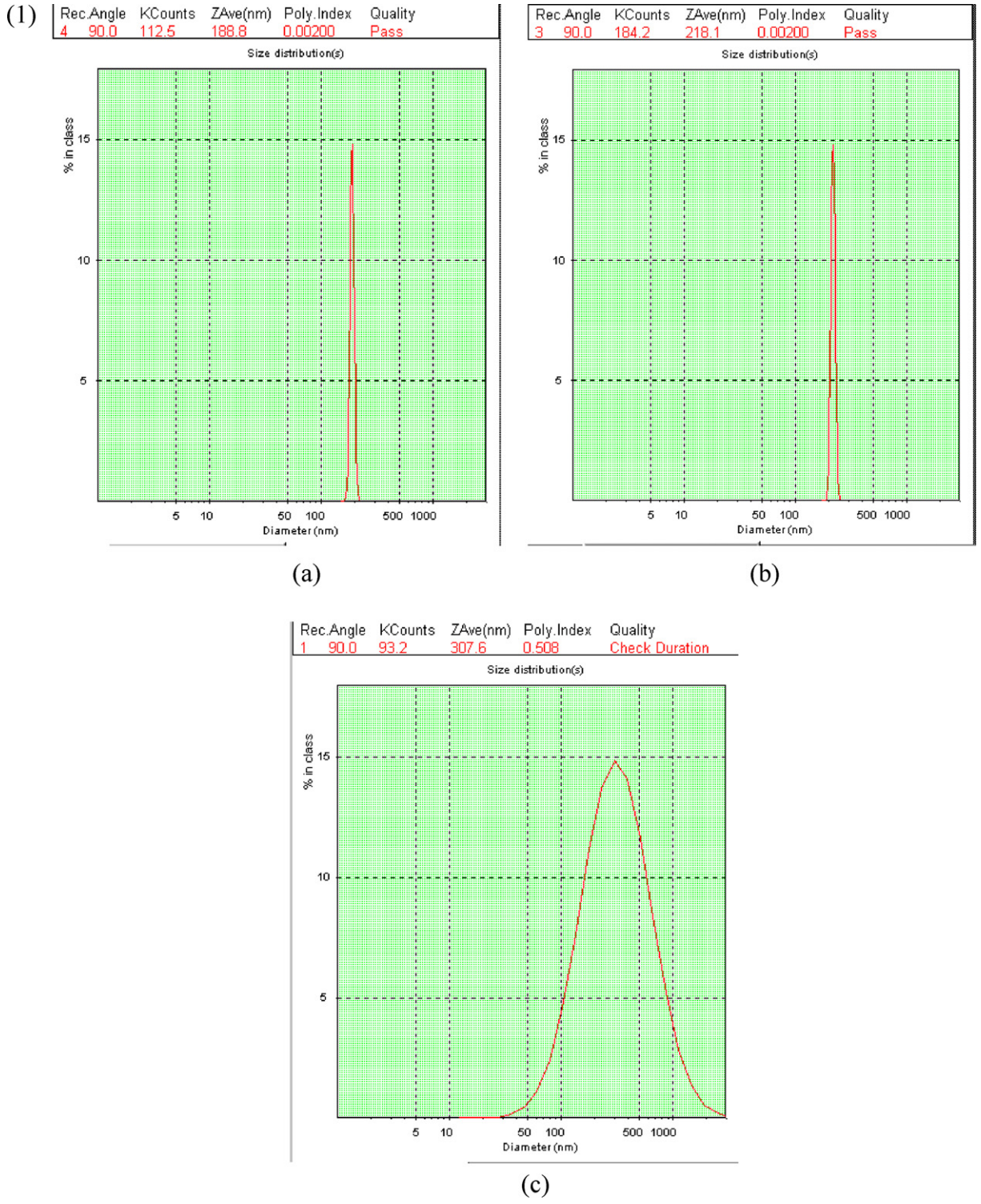

Fig. 3. (1) Particle size distribution, (2) FE-SEM images, (3) TEM images. P_{DDAB} = 0.08%; (a) $MW_{\gamma\text{-PGA}}$ = 6 kDa; (b) $MW_{\gamma\text{-PGA}}$ = 14 kDa; (c) $MW_{\gamma\text{-PGA}}$ = 52 kDa.

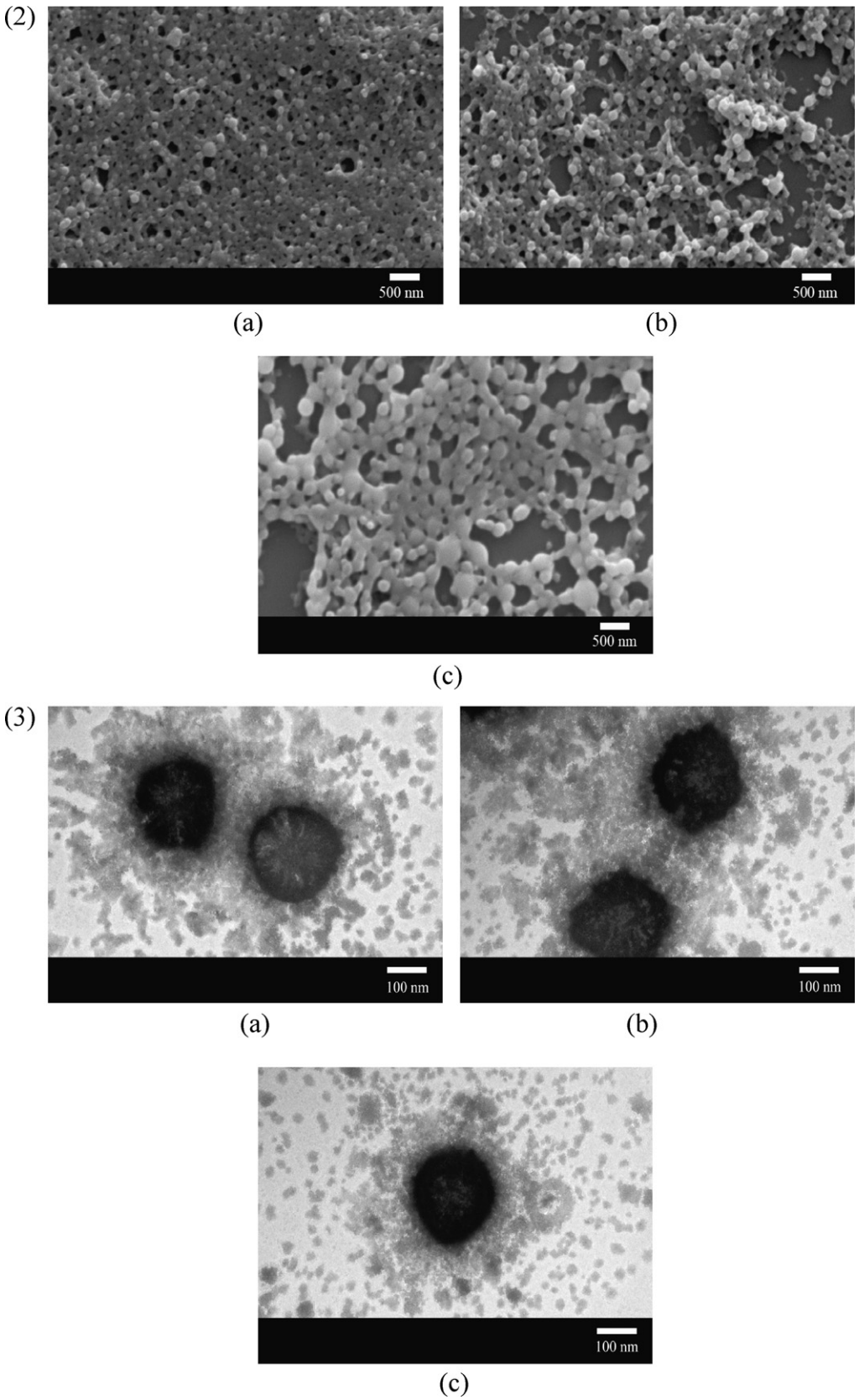

Fig. 3. (*continued*)

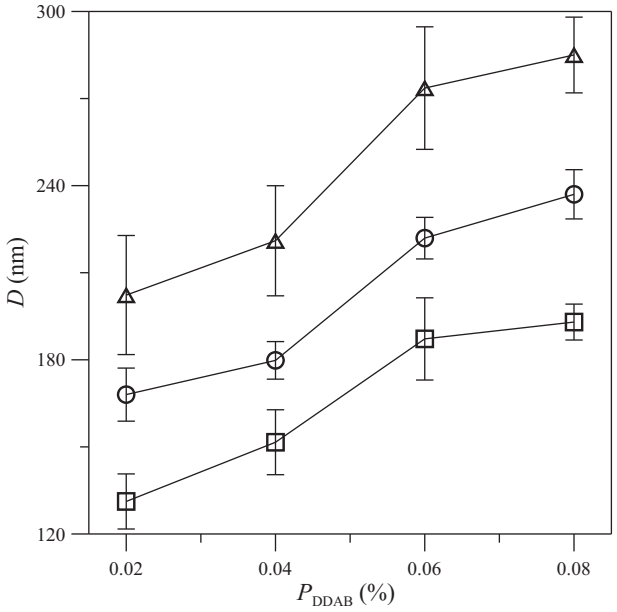

Fig. 4. Average particle diameter of γ-PGA/SQV-PLGA NPs. (△) $MW_{\gamma\text{-PGA}}$ = 52 kDa; (○) $MW_{\gamma\text{-PGA}}$ = 14 kDa; □) $MW_{\gamma\text{-PGA}}$ = 6 kDa. n = 3.

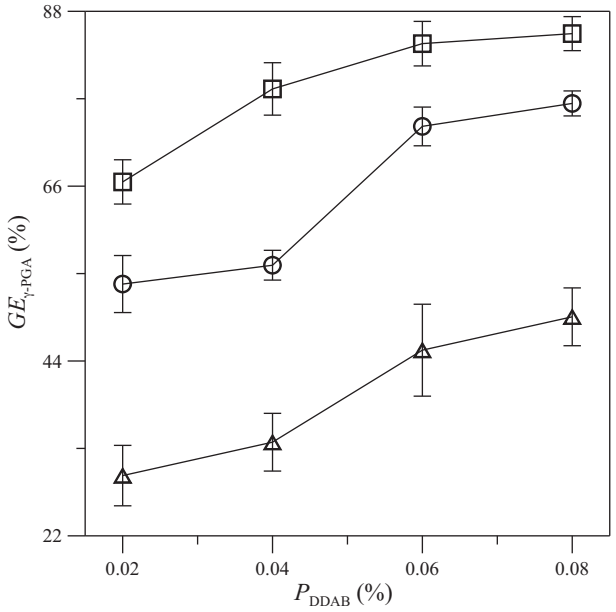

Fig. 6. Grafting efficiency of γ-PGA on SQV-PLGA NPs. (△) $MW_{\gamma\text{-PGA}}$ = 52 kDa; (○) $MW_{\gamma\text{-PGA}}$ = 14 kDa; (□) $MW_{\gamma\text{-PGA}}$ = 6 kDa. n = 3.

SQV-rich region in the peripheral shell of SQV-PLGA NPs. In addition, tiny pores emerged on the surface of SQV-PLGA NPs (Faisant et al., 2002; Klose et al., 2006). The pores accelerated the diffusion of SQV near the interface between SQV-PLGA NPs and γ-PGA. Following the first burst stage, the lag dissolution phase emerged with a characteristic of retarded and sustained release of SQV. This was because the agitation-derived fluid stress started to destroy the surface layer of γ-PGA on SQV-PLGA NPs (Kuo et al., 2011). In addition, the rate of hydrolysis for decomposing PLGA was constant in the lag phase (Faisant et al., 2006; Zolnik et al., 2006). Therefore, the degradation of PLGA controlled the release of SQV from the polymeric formulations. After the 22nd day, the release of SQV belonged to the secondary burst stage. This was because the bulk erosion of PLGA in γ-PGA/SQV-PLGA NPs demolished the ester bonds (–COO–) in the polymer backbone and produced lactic and glycolic acid (Raghuvanshi et al., 1993; Zolnik and Burgess, 2007). The two acidic monomers induced autocatalysis for further hydrolyzing PLGA, yielded the disintegration of particulate structure, and accelerated the dissolution of SQV (Wang et al., 2006). However, the third stage was not apparent in the case of modification with γ-PGA of 6 kDa. This was because SQV in this carrier system was close to depletion at the end of the second phase. Therefore, the driving force for accelerating release of SQV was feeble in the third stage (Kuo and Liang, 2011). As indicated in Fig. 8, the dissolution rate of SQV from γ-PGA/SQV-PLGA NPs was faster than that from SQV-PLGA NPs. This was because the hydrophilic γ-PGA could promote the penetration of water to the hydrophobic SQV-

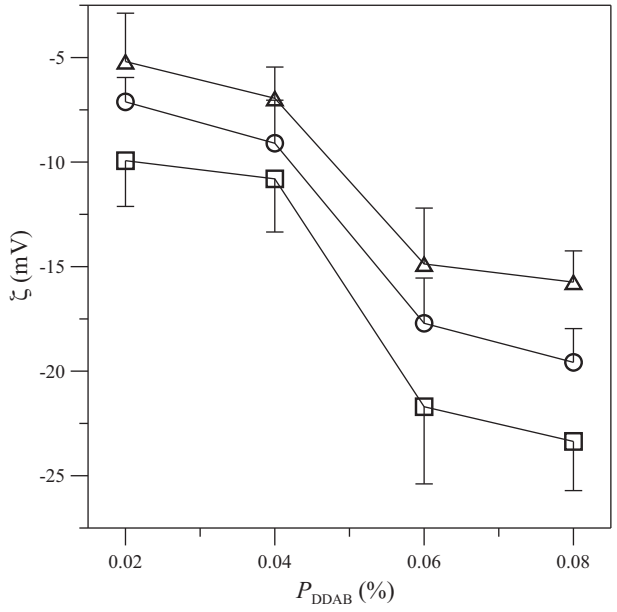

Fig. 5. Zeta potential of γ-PGA/SQV-PLGA NPs. (△) $MW_{\gamma\text{-PGA}}$ = 52 kDa; (○) $MW_{\gamma\text{-PGA}}$ = 14 kDa; (□) $MW_{\gamma\text{-PGA}}$ = 6 kDa. n = 3.

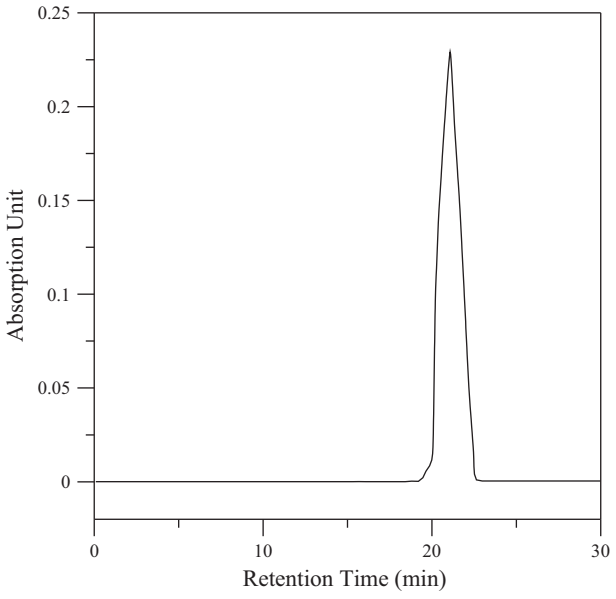

Fig. 7. GPC peak of γ-PGA/PLGA NPs with $MW_{\gamma\text{-PGA}}$ = 52 kDa.

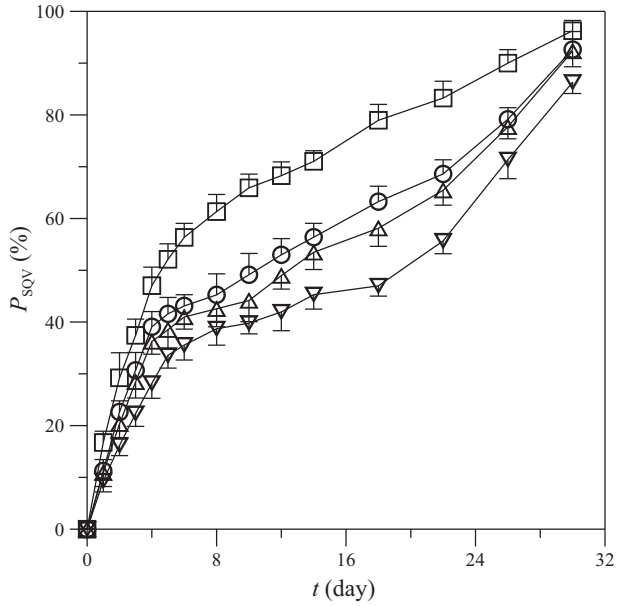

Fig. 8. Dissolution percentage of SQV from γ-PGA/SQV-PLGA NPs. P_{DDAB} = 0.08%. (△) $MW_{γ\text{-PGA}}$ = 52 kDa; (○) $MW_{γ\text{-PGA}}$ = 14 kDa; (□) $MW_{γ\text{-PGA}}$ = 6 kDa; (▽) SQV-PLGA NPs. n = 3.

PLGA NPs for surface and bulk erosion. In addition, an increment in the molecular weight of γ-PGA reduced the dissolution rate of SQV. This behavior could be attributed to the following two reasons. First, a higher molecular weight of γ-PGA yielded a lower quantity of the grafted γ-PGA on the particle surface (data shown in Fig. 6), rendering a weaker erosion effect. Second, a higher molecular weight of γ-PGA induced a higher level of chain entanglement and steric hindrance for releasing SQV (Tallury et al., 2008).

Fig. 9 shows the permeability of SQV across the monolayer of HBMEC/HA using γ-PGA/SQV-PLGA NPs as delivery vehicles. As displayed in this figure, the permeability of SQV across the BBB enhanced when the average grafting efficiency increased, in general. The rationale behind these results was described as follows.

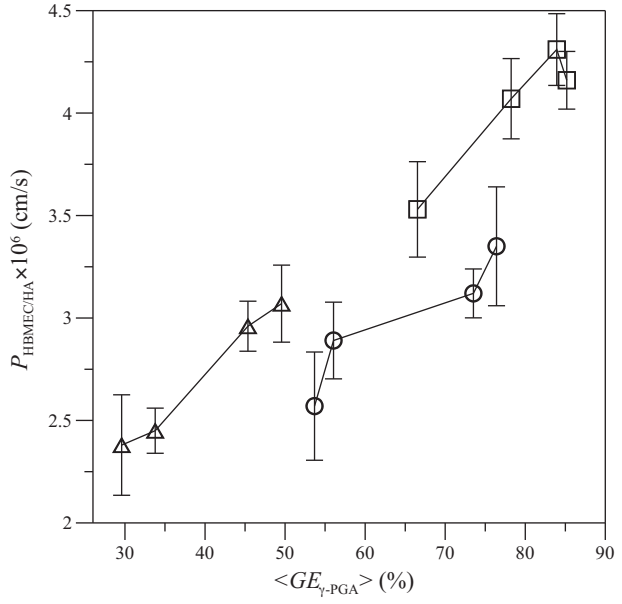

Fig. 9. Effect of the grafting efficiency of γ-PGA on the permeability of SQV in γ-PGA/SQV-PLGA NPs across the BBB constituted with HA-regulated HBMECs. (△) $MW_{γ\text{-PGA}}$ = 52 kDa; (○) $MW_{γ\text{-PGA}}$ = 14 kDa; (□) $MW_{γ\text{-PGA}}$ = 6 kDa. n = 3.

First, the grafting efficiency of γ-PGA on SQV-PLGA NPs was controlled by the concentration of DDAB (see Fig. 6). A higher grafting efficiency yielded a larger quantity of γ-PGA on SQV-PLGA NPs. Second, an increase in the quantity of γ-PGA enhanced the expression of ODC in HBMECs (images shown in Fig. 10). It was also observed that ODC promoted the permeability across the BBB via synthesis of polyamines (Poduslo and Curran, 1996). Third, SQV-PLGA NPs conjugated with a large quantity of γ-PGA improved the uptake of carriers via γ-PGA-specific receptor-mediated pathway (Kurosaki et al., 2010; Liang et al., 2005). Fourth, the uptake of γ-PGA/SQV-PLGA NPs by HBMECs was also regulated by γ-PGA-specific receptor-mediated process with energy-dependent characteristics (Kurosaki et al., 2009). As a result, γ-PGA played a critical role in improving the transport of SQV across the BBB via the enhanced permeability and retention effect (Li, 2002). However, an increase in the average grafting efficiency from 83.9 to 85.2% at 6 kDa slightly obstructed the transport of SQV, as displayed in Fig. 9. The reason was that the comparably large negative charge in this case (data shown in Fig. 5) yielded a strong electrical repulsion and high potential energy barrier between γ-PGA/SQV-PLGA NPs and HBMECs (Kuo and Wang, 2010; Ohshima, 2006). In addition, the permeability of free SQV was $(0.72 \pm 0.09) \times 10^{-6}$ cm/s in this study. Based on this datum, γ-PGA/SQV-PLGA NPs increased the permeability of SQV across the BBB about 3–6 times, as indicated in Fig. 9. The permeability of SQV loaded in NPs reached the maximum (increased about 6 times) when the average grafting efficiency was 83.9% and the molecular weight of γ-PGA was 6 kDa. Moreover, Fig. 9 associated with Fig. 6 suggested that a lower molecular weight of γ-PGA yielded a higher permeability of SQV at a constant concentration of DDAB. The following three reasons could explain this conclusion. First, a stimulation of the grafted γ-PGA promoted the activity of ODC in HBMECs (images shown in Fig. 10). Second, a lower molecular weight of γ-PGA produced a higher grafting efficiency, improved the specific ligand-receptor recognition of γ-PGA/SQV-PLGA NPs by HBMECs, and enhanced the permeability. Third, a lower molecular weight of γ-PGA yielded a slighter chain entanglement, a weaker steric hindrance, and a stronger uptake effect. In a study on the transport of fluorescent markers, it was observed that a maker with a low molecular weight could enhance the permeability across the BBB (Mark and Miller, 1999). In addition, we observed the interaction between HBMECs and HAs through the pores of the supporting PET membrane (Kuo and Lu, 2011a). HBMEC/HA could also reduce the uptake of calcein-AM and enhance the expression of P-glycoprotein and multidrug resistance-associated proteins on HBMECs (Kuo and Lu, 2011b).

Fig. 10 shows the uptake of γ-PGA/SQV-PLGA NPs by HBMECs and expression of ODC. When Fig. 10(a) was compared with (b), an increase in the grafting efficiency of γ-PGA (regulated by the doze of DDAB, see Fig. 6) enhanced the uptake of γ-PGA/SQV-PLGA NPs (green spots) and expression of ODC (red patches). The intensity of green fluorescence in Fig. 10(b) was 1.36 times that in Fig. 10(a). The red intensity in Fig. 10(b) was 1.21 times that in Fig. 10(a). In addition, the green and red intensity in Fig. 10(d) was, respectively, 1.29 and 1.42 times that in Fig. 10(c). The green and red intensity in Fig. 10(f) was, respectively, 1.21 and 1.69 times that in Fig. 10(e). As indicated in Fig. 10(a), (c), and (e), a decrease in molecular of γ-PGA enhanced the uptake of γ-PGA/SQV-PLGA NPs and expression of ODC. The same behavior was observed in Fig. 10(b), (d), and (f). These images supported the data shown in Fig. 9. The rationale behind the relation between the ODC expression and BBB permeability is described as follows. First, it has been observed that the expressed ODC could enhance the transport across the BBB (Poduslo and Curran, 1996). Second, an electromagnetic field (EMF) stimulated the synthesis of ODC (Farrell et al., 1998). An exposure to an EMF could also promote the endocytosis and permeability across the BBB (Mahrour et al., 2005; Oscar and Hawkins, 1977).

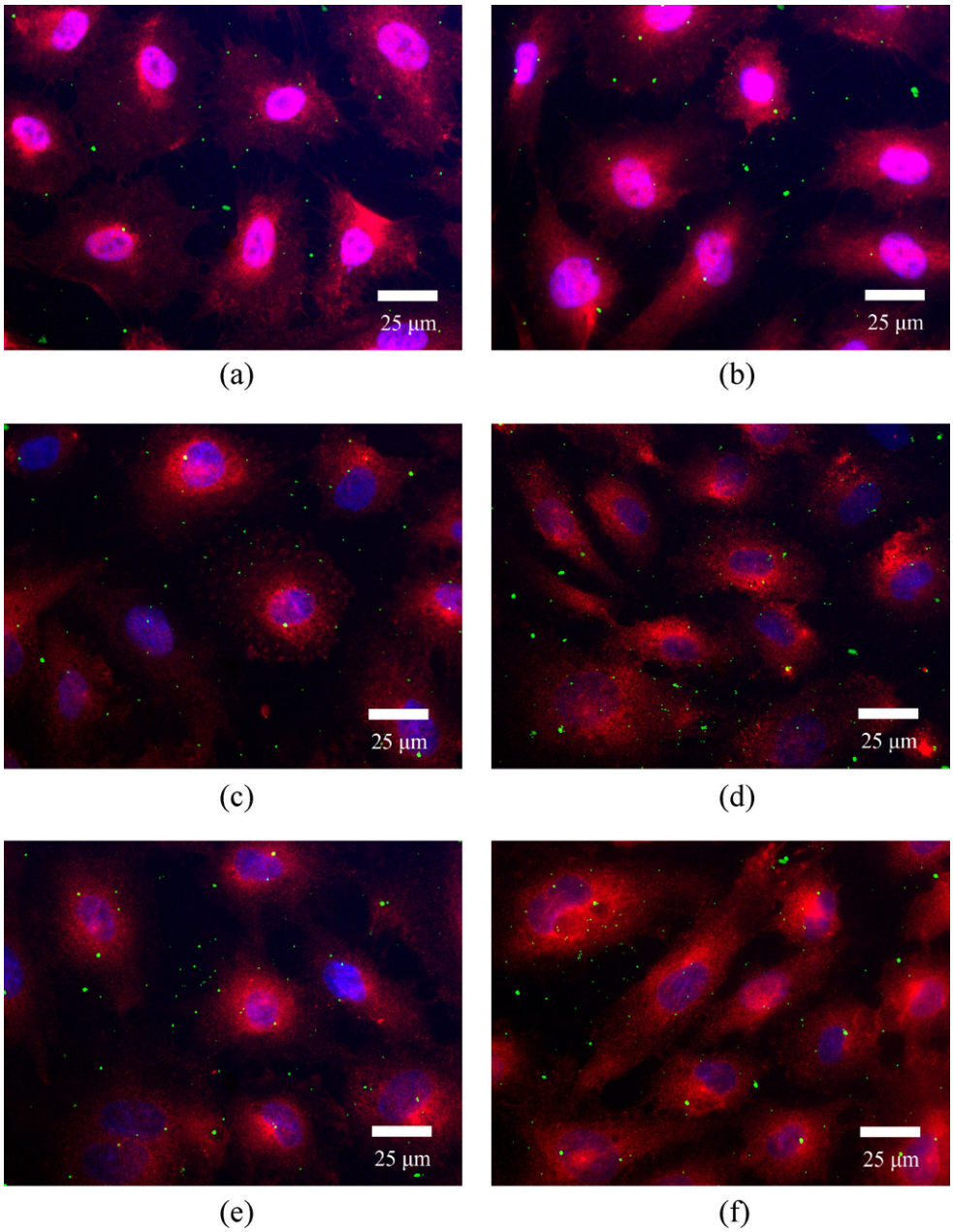

Fig. 10. Uptake of γ-PGA/SQV-PLGA NPs and expression of ODC. (a) $MW_{\gamma\text{-PGA}}$ = 52 kDa, P_{DDAB} = 0.02%; (b) $MW_{\gamma\text{-PGA}}$ = 52 kDa, P_{DDAB} = 0.08%; (c) $MW_{\gamma\text{-PGA}}$ = 14 kDa, P_{DDAB} = 0.02%; (d) $MW_{\gamma\text{-PGA}}$ = 14 kDa, P_{DDAB} = 0.08%; (e) $MW_{\gamma\text{-PGA}}$ = 6 kDa, P_{DDAB} = 0.02%; (f) $MW_{\gamma\text{-PGA}}$ = 6 kDa, P_{DDAB} = 0.08%.

Therefore, the expression of ODC could be considerably related to the delivery of γ-PGA/SQV-PLGA NPs across the BBB.

4. Conclusions

γ-PGA/SQV-PLGA NPs were fabricated to carry SQV across the BBB. An increase in the concentration of DDAB enhanced the particle size, absolute value of the zeta potential, and grafting efficiency of γ-PGA on SQV-PLGA NPs. In addition, an increment in the molecular weight of γ-PGA increased the size of γ-PGA/SQV-PLGA NPs. However, a larger molecular weight of γ-PGA reduced the absolute value of the zeta potential and grafting efficiency. The surface γ-PGA could promote the uptake of water and accelerate the release of SQV from γ-PGA/SQV-PLGA NPs. Moreover, an increment in the molecular weight of γ-PGA reduced the dissolution rate of SQV due to a reduced grafting quantity and an enlarged chain-entangling steric barrier. An increase in the grafting efficiency of γ-PGA by increasing the concentration of DDAB could improve the permeability of SQV across the monolayer of HBMEC/HA, in general, and so could a decrease in the molecular weight of γ-PGA. However, γ-PGA/SQV-PLGA NPs with a relatively high absolute value of the zeta potential reduced the permeability of SQV via electrical repulsion between the carriers and HBMECs. An increase in the quantity of γ-PGA enhanced the uptake of γ-PGA/SQV-PLGA NPs and expression of ODC by HBMECs.

Acknowledgment

This work is supported by the National Science Council of the Republic of China.

References

Akagi, T., Kaneko, T., Kida, T., Akashi, M., 2005. Preparation and characterization of biodegradable nanoparticles based on poly(g-glutamic acid) with L-phenylalanine as a protein carrier. J. Control. Release 108, 226–236.

Chung, T.H., Wu, S.H., Yao, M., Lu, C.W., Lin, Y.S., Hung, Y., Mou, C.Y., Chen, Y.C., Huang, D.M., 2007. The effect of surface charge on the uptake and biological function of mesoporous silica nanoparticles in 3T3-L1 cells and human mesenchymal stem cells. Biomaterials 28, 2959–2966.

Date, A.A., Joshi, M.D., Patravale, V.B., 2007. Parasitic diseases: liposomes and polymeric nanoparticles versus lipid nanoparticles. Adv. Drug Deliv. Rev. 59, 505–521.

Deeken, J.F., Löscher, W., 2007. The blood–brain barrier and cancer: transporters, treatment, and Trojan horses. Clin. Cancer Res. 13, 1663–1674.

Faisant, N., Akiki, J., Siepmann, F., Benoit, J.P., Siepmann, J., 2006. Effects of the type of release medium on drug release from PLGA-based microparticles: experiment and theory. Int. J. Pharm. 314, 189–197.

Faisant, N., Siepmann, J., Benoit, J.P., 2002. PLGA-based microparticles: elucidation of mechanisms and a new, simple mathematical model quantifying drug release. Eur. J. Pharm. Sci. 15, 355–366.

Faraji, A.H., Wipf, P., 2009. Nanoparticles in cellular drug delivery. Bioorg. Med. Chem. 17, 2950–2962.

Farrell, J.M., Barber, M., Krause, D., Litovitz, T.A., 1998. The superposition of a temporally incoherent magnetic field inhibits 60-Hz induced changes in the ODC activity of developing chick embryos. Bioelectromagnetics 19, 53–56.

Fasbender, A., Marshall, J., Moninger, T.O., Grunst, T., Cheng, S., Welsh, M.J., 1997. Effect of co-lipids in enhancing cationic lipid-mediated gene transfer in vitro and in vivo. Gene Ther. 4, 716–725.

Gaillard, P.J., de Boer, A.G., 2000. Relationship between permeability status of the blood–brain barrier and in vitro permeability coefficient of a drug. Eur. J. Pharm. Sci. 12, 95–102.

Glynn, S.L., Yazdanian, M., 1998. In vitro blood–brain barrier permeability of nevirapine compared to other HIV antiretroviral agents. J. Pharm. Sci. 87, 306–310.

Hans, M.L., Lowman, A.M., 2002. Biodegradable nanoparticles for drug delivery and targeting. Curr. Opin. Solid State Mater. Sci. 6, 319–327.

Irurzun, I., Bou, J.J., Camero, G.P., Abad, C., Campos, A., Guerra, S.M., 2001. Mark–Houwink parameters of biosynthetic poly(γ-glutamic acid) in aqueous solution. Macromol. Chem. Phys. 202, 3253–3256.

Ito, Y., Tanaka, T., Ohmachi, T., Asada, Y., 1996. Glutamic acid independent production of poly(γ-glutamic acid) by *Bacillus subtilis* TAM-4. Biosci. Biotechnol. Biochem. 60, 1239–1242.

Junghanns, J.U., Müller, R.H., 2008. Nanocrystal technology, drug delivery and clinical applications. Int. J. Nanomed. 3, 295–309.

Klose, D., Siepmann, F., Elkharraz, K., Krenzlin, S., Siepmann, J., 2006. How porosity and size affect the drug release mechanisms from PLGA-based microparticles. Int. J. Pharm. 314, 198–206.

Kreuter, J., 2005. Application of nanoparticles for the delivery of drugs to the brain. Int. Congr. Ser. 1277, 85–94.

Kreuter, J., 2001. Nanoparticulate systems for brain delivery of drugs. Adv. Drug Deliv. Rev. 47, 65–81.

Kunioka, M., Furusawa, K.J., 1997. Poly(γ-glutamic acid) hydrogel prepared from microbial poly(γ-glutamic acid) and alkane diamine with water-soluble carbodiimide. Appl. Polym. Sci. 65, 1889–1893.

Kuo, Y.C., Chiu, K.H., 2011. Inverted colloidal crystal scaffolds with laminin-derived peptides for neuronal differentiation of bone marrow stromal cells. Biomaterials 32, 819–831.

Kuo, Y.C., Chung, J.F., 2011. Physicochemical properties of nevirapine-loaded solid lipid nanoparticles and nanostructured lipid carriers. Colloids Surf. B 83, 299–306.

Kuo, Y.C., Liang, C.T., 2011. Inhibition of human brain malignant glioblastoma cells using carmustine-loaded catanionic solid lipid nanoparticles with surface anti-epithelial growth factor receptor. Biomaterials 32, 3340–3350.

Kuo, Y.C., Lin, P.I., Wang, C.C., 2011. Targeting nevirapine delivery across human brain microvascular endothelial cells using transferrin-grafted poly(lactide-co-glycolide) nanoparticles. Nanomedicine, in press, doi:10.2217/nnm.11.25.

Kuo, Y.C., Lu, C.H., 2011a. Effect of human astrocytes on the characteristics of human brain-microvascular endothelial cells in the blood–brain barrier. Colloids Surf. B 86, 225–231.

Kuo, Y.C., Lu, C.H., 2011b. Regulation of endocytosis into human brain-microvascular endothelial cells by inhibition of efflux proteins. Colloids Surf. B 87, 139–145.

Kuo, Y.C., Yu, H.W., 2011. Surface coverage of didecyl dimethylammonium bromide on poly(lactide-co-glycolide) nanoparticles. Colloids Surf. B 84, 253–258.

Kuo, Y.C., Wang, C.C., 2010. Electrophoresis of human brain microvascular endothelial cells with uptake of cationic solid lipid nanoparticles: effect of surfactant composition. Colloids Surf. B 76, 286–291.

Kuo, Y.C., Lin, C.W., 2009. Effect of electromagnetic field and surface modification on the electrical behavior of novel solid lipid nanoparticles covered with L-arginine. Colloids Surf. B 71, 45–51.

Kuo, Y.C., Yeh, C.F., Yang, J.T., 2009. Differentiation of bone marrow stromal cells in poly(lactide-co-glycolide)/chitosan scaffolds. Biomaterials 30, 6604–6613.

Kuo, Y.C., Kuo, C.Y., 2008. Electromagnetic interference in the permeability of saquinavir across the blood–brain barrier using nanoparticulate carriers. Int. J. Pharm. 351, 271–281.

Kuo, Y.C., Lin, S.C., 2008. Effect of glutamate on the electrical properties of cationic solid lipid nanoparticles containing stearylamine and dioctadecyldimethyl ammonium bromide. J. Phys. Chem. B 112, 4454–4460.

Kuo, Y.C., Chen, I.C., 2007. Evaluation of surface charge density and surface potential by electrophoretic mobility for solid lipid nanoparticles and human brain-microvascular endothelial cells. J. Phys. Chem. B 111, 11228–11236.

Kuo, Y.C., Chen, H.H., 2006. Effect of nanoparticulate polybutylcyanoacrylate and methylmethacrylate-sulfopropylmethacrylate on the permeability of zidovudine and lamivudine across the in vitro blood–brain barrier. Int. J. Pharm. 327, 160–169.

Kuo, Y.C., Lin, T.W., 2006. Electrophoretic mobility, zeta potential, and fixed charge density of bovine knee chondrocytes, methylmethacrylate-sulfopropylmethacrylate, polybutylcyanoacrylate, and solid lipid nanoparticles. J. Phys. Chem. B 110, 2202–2208.

Kuo, Y.C., 2005. Loading efficiency of stavudine on polybutylcyanoacrylate and methylmethacrylate-sulfopropylmethacrylate copolymer nanoparticles. Int. J. Pharm. 290, 161–172.

Kuo, Y.C., Chung, C.Y., 2005. Transport of zidovudine- and lamivudine-loaded polybutylcyanoacrylate and methylmethacrylate-sulfopropylmethacrylate nanoparticles across the in vitro blood–brain barrier: characteristics of the drug-delivery system. J. Chin. Inst. Chem. Eng. 36, 627–638.

Kurosaki, T., Kitahara, T., Kawakami, S., Higuchi, Y., Yamaguchi, A., Nakagawa, H., Kodama, Y., Hamamoto, T., Hashida, M., Sasaki, H., 2010. γ-Polyglutamic acid-coated vectors for effective and safe gene therapy. J. Control. Release 142, 404–410.

Kurosaki, T., Kitahara, T., Fumoto, S., Nishida, K., Nakamura, J., Niidome, T., Kodama, Y., Nakagawa, H., To, H., Sasaki, H., 2009. Ternary complexes of pDNA, polyethylenimine, and γ-polyglutamic acid for gene delivery systems. Biomaterials 30, 2846–2853.

Langer, K., Marburger, C., Berthold, A., Kreuter, J., Stieneker, F., 1996. Methylmethacrylate sulfopropylmethacrylate copolymer nanoparticles for drug delivery: preparation and physicochemical characterization. Int. J. Pharm. 137, 67–74.

Li, C., 2002. Poly(L-glutamic acid)-anticancer drug conjugates. Adv. Drug Deliv. Rev. 54, 695–713.

Liang, H.F., Yang, T.F., Huang, C.T., Chen, M.C., Sung, H.W., 2005. Preparation of nanoparticles composed of poly(γ-glutamic acid)-poly(lactide) block copolymers and evaluation of their uptake by HepG2 cells. J. Control. Release 105, 213–225.

Mahrour, N., Pologea-Moraru, R., Moisescu, M.G., Orlowski, S., Levêque, P., Mir, L.M., 2005. In vitro increase of the fluid-phase endocytosis induced by pulsed radiofrequency electromagnetic fields: importance of the electric field component. Biochim. Biophys. Acta 1668, 126–137.

Makino, K., Yamamoto, S., Fujimoto, K., Kawaguchi, H., Ohshima, H., 1994. Surface structure of latex particles covered with temperature-sensitive hydrogel layers. J. Colloid Interface Sci. 166, 251–258.

Mark, K.S., Miller, D.W., 1999. Increased permeability of primary cultured brain microvessel endothelial cell monolayers following TNF-α exposure. Life Sci. 64, 1941–1953.

Ohshima, H., 2006. Electrophoresis of soft particles: analytic approximations. Electrophoresis 27, 526–533.

Okamoto, S., Matsuura, M., Akagi, T., Akashi, M., Tanimoto, T., Ishikawa, T., Takahashi, M., Yamanishi, K., Mori, Y., 2009. Poly(glutamic acid) nanoparticles combined with mucosal influenza virus hemagglutinin vaccine protects against influenza virus infection in mice. Vaccine 27, 5896–5905.

Oscar, K.J., Hawkins, T.D., 1977. Microwave alteration of the blood–brain barrier system of rats. Brain Res. 126, 281–293.

Pardridge, W.M., 2005. The blood–brain barrier: bottleneck in brain drug development. J. Am. Soc. Exp. NeuroTher. 2, 3–14.

Peng, S.F., Yang, M.J., Su, C.J., Chen, H.L., Lee, P.W., Wei, M.C., Sung, H.W., 2009. Effects of incorporation of poly(γ-glutamic acid) in chitosan/DNA complex nanoparticles on cellular uptake and transfection efficiency. Biomaterials 30, 1797–1808.

Poduslo, J.F., Curran, G.L., 1996. Increased permeability of superoxide dismutase at the blood–nerve and blood–brain barriers with retained enzymatic activity after covalent modification with naturally occurring polyamine, putrescine. J. Neurochem. 67, 734–741.

Raghuvanshi, R.S., Singh, M., Talwar, G.P., 1993. Biodegradable delivery system for single step immunization with tetanus toxoid. Int. J. Pharm. 93, 1–5.

Schroeder, U., Sommerfeld, P., Sabel, B.A., 1998. Efficacy of oral dalargin-loaded nanoparticle delivery across the blood–brain barrier. Peptides 19, 777–780.

Sonorhara, R., Muramatsu, N., Ohshima, H., Kondo, T., 1995. Difference in surface properties between *Escherichia coli* and *Staphylococcus aureus* as revealed by electrophoretic mobility measurement. Biophys. Chem. 55, 273–277.

Tallury, P., Airrabeelli, R., Li, J., Paquette, D., Kalachandra, S., 2008. Release of antimicrobial and antiviral drugs from methacrylate copolymer system: effect of copolymer molecular weight and drug loading on drug release. Dent. Mater. 24, 274–280.

Wang, X., Venkatraman, S.S., Boey, Y.C., Loo, S.C., Tan, L.P., 2006. Controlled release of sirolimus from a multilayered PLGA stent matrix. Biomaterials 27, 5588–5595.

Yoshikawa, T., Okada, N., Oda, A., Matsuo, K., Matsuo, K., Kayamuro, H., Ishii, Y., Yoshinaga, T., Akagi, T., Akashi, M., Nakagawa, S., 2008. Nanoparticles built by self-assembly of amphiphilic γ-PGA can deliver antigens to antigen-presenting cells with high efficiency: a new tumor-vaccine carrier for eliciting effector T cells. Vaccine 26, 1303–1313.

Zolnik, B.S., Burgess, D.J., 2007. Effect of acidic pH on PLGA microsphere degradation and release. J. Control. Release 122, 338–344.

Zolnik, B.S., Leary, P.E., Burgess, D.J., 2006. Elevated temperature accelerated release testing of PLGA microspheres. J. Control. Release 112, 293–300.